Relating ionization quenching in organic plastic scintillators to basic material properties by modelling excitation density transport and amorphous track structure during proton irradiation

Christensen, Jeppe Brage; Andersen, Claus E.

Published in:
Physics in Medicine and Biology

Link to article, DOI:
10.1088/1361-6560/aadf2d

Publication date:
2018

Document Version
Peer reviewed version

Relating ionization quenching in organic plastic scintillators to basic material properties by modelling excitation density transport and amorphous track structure during proton irradiation

Jeppe Brage Christensen and Claus E. Andersen

Center for Nuclear Technologies, Technical University of Denmark,
Frederiksborgvej 399, 4000 Roskilde, Denmark
jepb@dtu.dk

Abstract

Ionization quenching in organic scintillators is usually corrected with methods that require careful assessment of the response relative to that of an ionization chamber. Here, we present a framework to compute ionization quenching correction factors (QCFs) from first principles for organic plastic scintillators exposed to ions. The tool solves the kinetic Blanc equation, of which the Birks model is a simplified solution, based on amorphous track structures models. As a consequence, ionization quenching correction factors can be calculated relying only on standard, tabulated scintillator material properties such as the density, light yield, and decay time.

The tool is validated against experimentally obtained QCFs for two different organic plastic scintillators irradiated with protons with linear energy transfers (LETs) between 5 and 70 MeV cm^{-1}. The QCFs computed from amorphous track structure models and the BC-400 scintillator properties deviate less than 3 % from the Birks model for LETs below 45 MeV cm^{-1} and less than 5 % for higher LETs. The agreement between experiments and the software for the BCF-12 scintillator is within 2 % for LETs below 45 MeV cm^{-1} and within 10 % for LETs above, comparable to the experimental uncertainties. The framework is compiled into the open source software `ExcitonQuenching` available for download. `ExcitonQuenching` enables computations of QCFs in organic plastic scintillators exposed to ions independently of experimentally based quenching parameters in contrast to the Birks model. `ExcitonQuenching` can improve the accuracy of correction factors and understanding of ionization quenching in scintillator dosimetry.

Keywords: Ionization quenching, organic scintillators, proton therapy, quenching kinetics, dosimetry

1 Introduction

Organic plastic scintillators are attractive for particle dosimetry due to the prompt response, small size, and good water-equivalence (Beddar et al., 1992a,b). Fibre-coupled scintillators are known to exhibit a stem-effect, where light is emitted outside the primary scintillating mechanism (Archambault et al., 2005; Therriault-Proulx et al., 2011), as well as a temperature dependence (Buranurak et al., 2013; Wootton and Beddar, 2013). These mechanisms are however well-understood and the effects can be corrected for. The situation for organic scintillators exposed to radiation with high linear energy transfer (LET) is more complex, and the reduced scintillator response, due to high local ionization densities, is termed ionization quenching. The quenching is traditionally explained as a reduction of the primary scintillation efficiency, where zones with a high ionization density fail to transfer all energy to the excited states (Birks, 1951). Kallmann and Brucker (1957) showed that most quenching occurs faster than the characteristic decay time of the scintillator, which may be explained in terms migration of excited states, heat conduction, and ionic recombination (Birks, 1964; Beddar and Beaulieu, 2016). The quenching is often corrected by comparing the response of the quenched signal in an organic scintillator to the unquenched signal measured with an ionization chamber. On the other hand, Alsanea et al. (2018) exploited the quenching differences in four organic scintillators to simultaneously measure the LET and dose in therapeutic proton beams. Monte Carlo simulations of the LET distribution enable quenching corrections by applying the semi-empirical formula developed by Birks (1951), henceforth referred to as the Birks model. Nonetheless, such quenching corrections often give rise to deviations up to 10 % at the Bragg peak due to the sharp LET-gradient (Beddar and Beaulieu, 2016).

Recently, Boivin et al. (2016) showed how the Birks model breaks down for high-LET photon beams, whereas a shortcoming for ions has been known for decades; two ions with same LET but different atomic number will in the Birks model give rise to the same ionization quenching. Such a prediction however contradicts experiments (Newman and Steigert, 1960; Birks, 1964) as the radial energy deposition by secondary electrons (EDSE) differs in the two cases. In any case, it motivates new approaches and the application of track structure models to account for the energy deposition by secondary electrons.

Blanc et al. (1962, 1964) developed a kinetic model where the energy of excited molecules is migrating radially and lost by fluorescence and quenching. The Blanc depends on—like the Birks model and most EDSE models—the

number of molecules involved in the quenching process. In this work, we focus on computing the ionization quenching for organic plastic scintillators based on the Blanc model. The Birks model itself takes on the form of a simplified version of the Blanc model (Birks, 1964, p. 198). As such, the Blanc formalism enables a more exact computation of the quenching correction factors than the Birks model and, furthermore, is independent of experimentally determined quenching parameters as the Birks kB factor.

Here, we use amorphous track structure theory to model the radial energy deposition after an ion has penetrated an organic plastic scintillator. Amorphous track structure theory often distinguishes between the core and the penumbra. The core is an extremely narrow zone with an enormous density of energy deposited by the incident ion whereas the penumbral region, exhibiting a r^{-2} density decrease, is mainly due to energy deposition by secondary electrons. The kinetic Blanc model is subsequently applied to evolve the initial radial energy deposition in the temporal and spatial domains while keeping track of the fluorescence and quenching. The Blanc model as a consequence is able to distinguish the quenching between two particles, with the same LET but different atomic numbers, in contrast to the Birks model.

The first part of the present work outlines the concepts of quenching corrections factors and track structure models. Solutions to the Blanc model are subsequently investigated with its inherent free parameters. The Blanc model consists of a set of general parameters, which in this work are estimated by fitting the Blanc model to experimentally obtained quenching correction factors. These parameters are then examined by computing the ionization quenching in a different scintillator and subsequently comparing the theory to experimental results.

The numerical framework to apply track structure theory and subsequently solve the Blanc equation is compiled into the open source code `ExcitonQuenching` available for download[1]. `ExcitonQuenching` computes the quenching correction factors from first principles using merely the density, decay time, and light yield of an organic plastic scintillator and the energy of the primary particle.

2 Background

2.1 Ionization quenching

The scintillation light yield per unit length $\mathrm{d}S/\mathrm{d}x$ for an organic scintillator is traditionally written in the form

$$\frac{\mathrm{d}S}{\mathrm{d}x} = \frac{A \cdot \mathrm{LET}}{\mathrm{QCF}}, \qquad \mathrm{QCF} = 1 + kB \cdot \mathrm{LET} + C \cdot \mathrm{LET}^2 + \cdots, \tag{1}$$

where A is the scintillation efficiency, and the Quenching Correction Factor (QCF) depends on the quenching parameters kB and C. The Birks model truncates the series at the first-order LET-term, which has been shown to be successfully applicable for quenching corrections (Beddar and Beaulieu, 2016). The second-order LET term was suggested by Chou (1952) and is often neglected but has been shown to give a better correction for high-LET (Torrisi, 2000).

2.2 Kinetics of excitation densities

Blanc et al. (1962, 1964) proposed a kinetic model which considers a number of molecules excited to the first singlet state which are allowed to migrate, fluoresce, and quench. The excited states are henceforth referred to as excitons to comply with the terminology in Birks (1964). The Blanc model governs the kinetics of the excitation density $n(r, t)$, where r is the distance from the centre of the ion track and t is the time after the ionization. The model takes on the form of (Blanc et al., 1962, 1964; Birks, 1964)

$$\frac{\partial n}{\partial t} = D\nabla^2 n - (p + k)n - \alpha n^2 - \beta n^3, \tag{2}$$

where D is the exciton diffusion constant, and p, k, αn, and βn^2 are defined as the rates of fluorescence emission, and uni-, bi-, and trimolecular quenching, respectively. Unimolecular quenching is isolated to a single molecule, whereas the importance of the bi- and tri-molecular quenching terms increases with the local exciton density, i.e. with increasing LET.

Consider two scintillators with the same density and decay time but different scintillation efficiencies being penetrated by two identical particles. The scintillator with the higher scintillation efficiency will thus have a larger local excitation density. As a consequence, the second- and third-order quenching terms will lead to more quenching

[1] `https://github.com/jbrage/ExcitonQuenching`

than in the scintillator with a lower scintillation efficiency. Similarly, two scintillators with the same scintillation efficiency and density—but different decay times—will require different quenching correction factors: Although the local exciton densities immediately after the particle passed are equal, the scintillator with the faster decay time is more efficient in emitting photons before they are quenched than the other. The diffusion term, on the other hand, causes the excitons to migrate away from the center of the particle track and hence decreases the quenching but not the rate of fluorescence emission. The Blanc model is an interesting ionization quenching model for several reasons:

1. The Blanc model corresponds to the Birks model if only fluorescence and unimolecular quenching are included (Birks, 1964, p. 198; Blanc et al., 1962), i.e. truncating eq. (1) at the first-order LET term.

   If fluorescence, uni-, and bimolecular quenching terms are included in the Blanc model, it corresponds to the model proposed by Chou (1952), i.e. with both kB and C as quenching parameters in eq. (1) (Birks, 1964, p. 198).

2. The Blanc model enables an inclusion of amorphous track structure theory, and—in contrast to the semi-empirical Birks and Chou models—two ions with same LET and different charges will hence give rise to different quenching correction factors as experimentally observed.

3. The solution of eq. (2) makes it feasible to examine the temporal structure of the ionization quenching.

The version of the Blanc equation in eq. (2) only models the exciton interactions between the first singlet state and the ground state. An extension to the equation, including the interactions with the first triplet state, could be added with a second coupled partial differential equation as suggested by Blanc et al. (1962). The extended model can be validated against experimentally obtained QCFs for an appropriate scintillator (e.g. BCF-60, Saint-Gobain, France, as measured by Hoehr et al. (2018)). Nonetheless, such a study is beyond the scope of this work.

2.3 Amorphous track structure models

The radial excitation density distribution in an ion track should vary according to the material and the energy of the primary particle and this can be achieved through amorphous track structure models. Amorphous track structures consider the radial energy distribution as the average of many secondaries and tracks, i.e. a continuous function, in contrast to the microdosimetric approach, where the stochastic nature of energy deposition by single electrons is taken into account. The initial number of excitations per unit length N_0 depends on the scintillation efficiency A, the number of photons emitted per deposited energy, as

$$N_0 = A \cdot \mathrm{LET}. \tag{3}$$

The ionization quenching is investigated using three different radial energy deposition distributions, namely the Gaussian (Blanc et al., 1964), Chatterjee-Schaefer (Chatterjee and Schaefer, 1976), and Scholz-Kraft (Scholz and Kraft, 1996) track structure models. The three track structure models are defined in appendix A and shown in figure 1 for two different energies.

The track structure models have been chosen to reflect the cases of (i) an extremely dense core (Chatterjee-Schaefer), (ii) the continuous transition from core to penumbra (Scholz-Kraft), and (iii) the Gaussian which is independent of the range of secondary electrons but has been applied historically due to its simplicity. Other track structure models, such as those by Hansen and Olsen (1984), Kiefer and Straaten (1986) and Katz and Varma (1991), could have been included as well with similar arguments.

The distribution of exciton densities using amorphous track structure models, and exciton interaction probabilities in terms of the Blanc model, makes it feasible to investigate ionization quenching at the macroscopic scale.

3 Methods

3.1 Experimentally determined quenching correction factors

Often the LET-varying QCF is estimated by comparing the quenched scintillator measurement to an unquenched measurement with an ionization chamber. Two such examples are shown in figure 2 where Wang et al. (2012) irradiated an organic fibre-coupled scintillator (BCF-12, Saint-Gobain, France) and Torrisi (2000) irradiated a thin organic scintillator (BC-400, Bicron, USA) with protons at different energies.

Wang et al. (2012) and Torrisi (2000) fitted the Birks model to the QCF as a function of LET which in both cases show an agreement within 5 %. Since the QCFs in both data sets are given for a wide LET range and differ by more than a factor of 2, they may serve as a reference and are applicable to validate the QCFs calculated with the

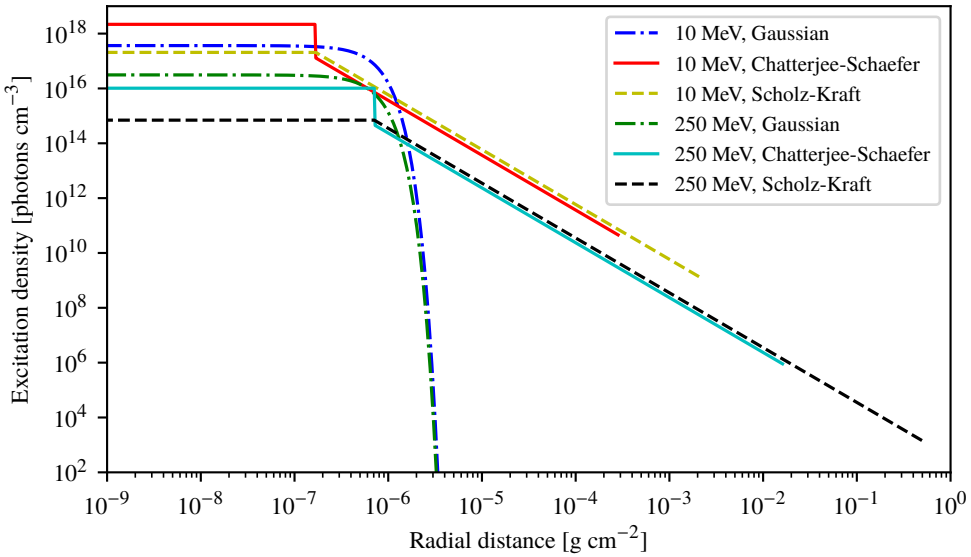

Figure 1: The three track structure models in equations (5), (6), and (8) for protons at 10 MeV and 250 MeV in water. The range of the secondary electrons depends on the kinetic energy of the primary particle, which is included in the Scholz-Kraft and Chatterjee-Schaefer track structures, but unaccounted for in the Gaussian model.

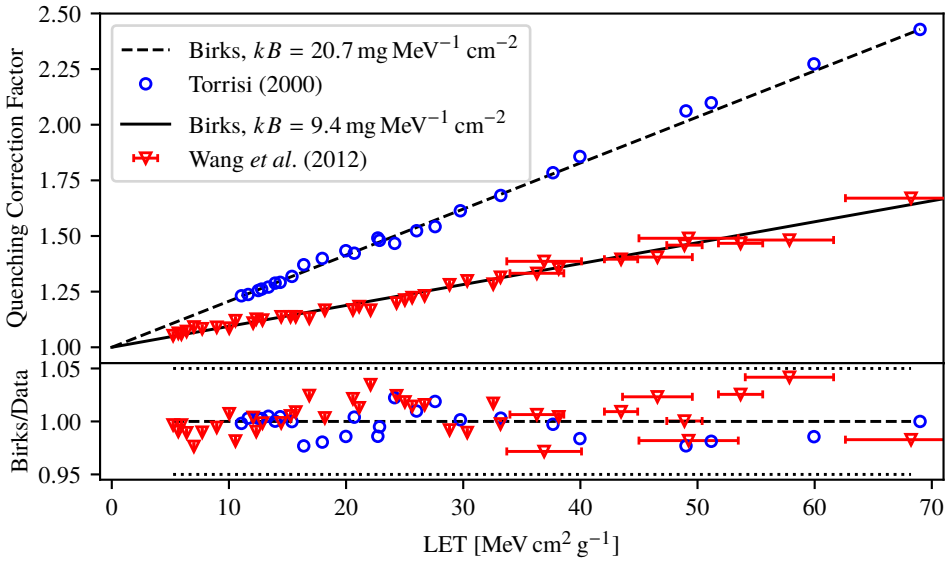

Figure 2: The quenching correction factor as a function of LET for two different organic scintillators irradiated with protons where the Birks model is fitted to the data in both cases. The ratios of the QCF obtained from the Birks model to the experimentally obtained values in the figure below indicate a good agreement for both measurements.

Blanc model. The parameters relevant for the Blanc model are listed in table 1 for the BC-400 and BCF-12 plastic scintillators.

Table 1: The scintillator parameters required to model the exciton densities and fluorescence emission are tabulated for most scintillators. The relevant parameters for the two scintillators in the present work are given below. Data from Saint-Gobain (2018).

Scintillator	Scintillation efficiency, A [photons/MeV]	Decay time τ [ns]	Density ρ [g cm^{-3}]
BCF-12	8,000	3.2	1.05
BC-400	11,300	2.4	1.03

3.2 Numerical scheme

The itinerary to quenching correction factors

The Blanc model is used to compute the QCF for a particle with energy E as outlined in figure 3. The scintillator efficiency A defines, along with the LET, the total number of excitons N_0 involved in the quenching process as given by eq. (3). The N_0 excitons are distributed radially according to an amorphous track structure model, where the penumbra and core radii are computed from the particle energy E and the density ρ of the scintillating material as given in appendix A. The chosen track structure model governs in any case the radial exciton distribution at time $t = 0$.

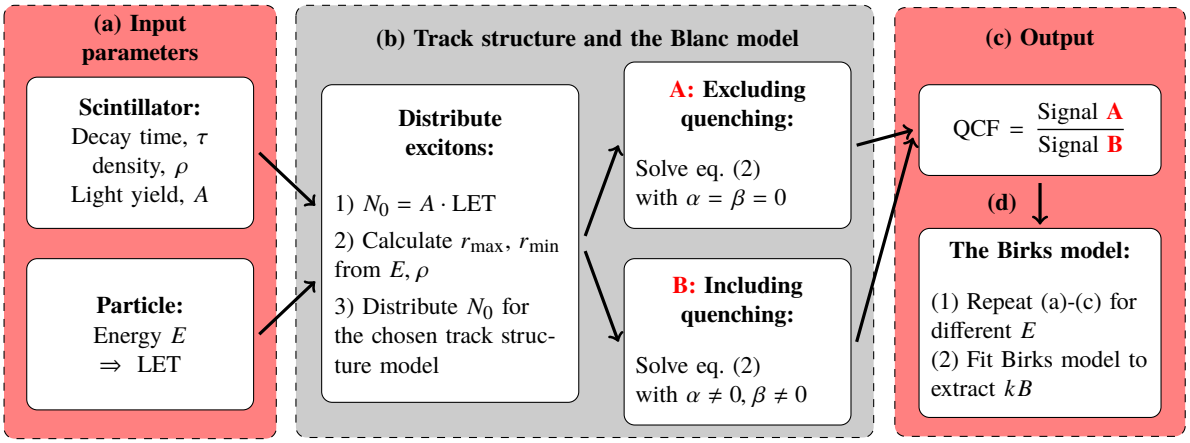

Figure 3: The workflow to a quenching correction factor. (a) The input parameters are responsible for the number of excitons involved in the quenching process. (b) The initial exciton distribution is modelled by the selected track structure model. The Blanc model in eq. (2) is subsequently used to calculate the emission of fluorescence in two cases: With and without ionization quenching. (c) The QCF is as a result computed as the ratio of the unquenched to the quenched signal. (d) The Birks model parameter kB can be calculated from a fit to a series of the QCFs as a function of LET.

The excitons are subsequently evolved in the temporal and spatial domain as governed by the Blanc model in eq. (2). The total emission of fluorescence photons, the signal, is computed by integrating over the fluorescence term pn in eq. (2) from time $t = 0$ to $t = \infty$. The numerical scheme used to solve the partial differential equation (2) is included in appendix B.

The QCF is computed by solving eq. (2) twice as outlined in figure 3 part (b); with and without the ionization quenching parameters. Setting the parameters $\alpha = \beta = 0$ in eq. (2) leads to a solution of the form $n(t) \propto \exp(-t/\tau)$, i.e. the fluorescence signal follows an exponential decay with time constant τ without ionization quenching. The solution to eq. (2) with $\alpha \neq 0, \beta \neq 0$, and thus including ionization quenching, reduces in any case the total signal. The QCF is accordingly computed as the ratio of the two signals. The steps (a)–(c) may be repeated for several particle

energies to plot the QCF as a function of LET. The Birks quenching parameter kB can consequently be extracted theoretically by fitting the Birks model to these computed data.

Quenching parameters in the Blanc model

The data by Wang et al. (2012) in figure 2 comprises the QCFs for protons penetrating the BCF-12 scintillator over a wide range of LETs, which can be used to determine the general (D, α, β) parameters in the Blanc model, eq. (2). The QCF for a particular plastic scintillator and particle in the Blanc formulation merely depends on the input parameters listed in figure 3(a). The scintillator decay time $\tau = (p + k)^{-1}$ is tabulated for most plastic scintillators, where the probability rates for the fluorescence emission p and unimolecular quenching k are weighted equally. Any weight cancels out as the QCF, figure 3(c), is computed as the ratio between the signals.

Let a proton with a given LET penetrate a thin BCF-12 layer where the excited states are radially distributed as in the, say, Scholz-Kraft model. The modified Blanc model in eq. (2) will then for one set of (D, α, β) parameters give rise to some QCF using the workflow outlined in figure 3. This calculation is repeated for all LET values present in the data set by Wang et al. (2012). The quality of the particular set of (D, α, β) parameters is evaluated through the sum of squares

$$\chi^2 = \sum_i \frac{(\mathrm{QCF}_{\mathrm{Blanc},i} - \mathrm{QCF}_{\mathrm{exp},i})^2}{\mathrm{QCF}_{\mathrm{exp},i}}, \qquad \forall i \in [\text{LET values in figure 2}] \tag{4}$$

where $\mathrm{QCF}_{\mathrm{Blanc},i}$ is the QCF computed with the Blanc model for the i'th LET-value in the Wang et al. (2012) data, and $\mathrm{QCF}_{\mathrm{exp},i}$ is the corresponding QCF obtained experimentally. The best set of (D, α, β) parameters is found by minimizing χ^2.

The exciton diffusivity has been experimentally estimated to be of the order of $D \simeq 5 \times 10^{-4}\,\mathrm{cm^2\,s^{-1}}$ (Kallmann and Brucker, 1957). The bimolecular quenching parameter is computed to be $\alpha \simeq 3.2 \times 10^{-9}\,\mathrm{cm^3\,s^{-1}}$ (Birks, 1964, p. 199), whereas the order of the trimolecular quenching parameter is to be determined. The uncertainties on the experimentally obtained values of D and α are unknown and they merely serve as means to compare to the computed χ^2 minima.

After the unique (D, α, β) parameters in the Blanc model have been established, the same parameters are used to compute the QCFs for protons interaction with the BC-400 scintillator and assessed against the corresponding experimental data by Torrisi (2000).

4 Results

4.1 Quenching parameters

The second-order Blanc equation

The roles of the diffusion constant D and the bimolecular quenching parameter α in the Blanc model are investigated by truncating eq. (2) after the second-order term, i.e. setting $\beta = 0$. χ^2 is in figure 4 mapped for various (α, D) pairs for the three track structure models in question. The (α, D) pairs are sampled uniformly over the given ranges 2000 times, and the χ^2 minimum is found by cubic interpolation. The experimentally determined D and calculated α values, listed in table 2, are marked with a cross in each χ^2 map for comparison.

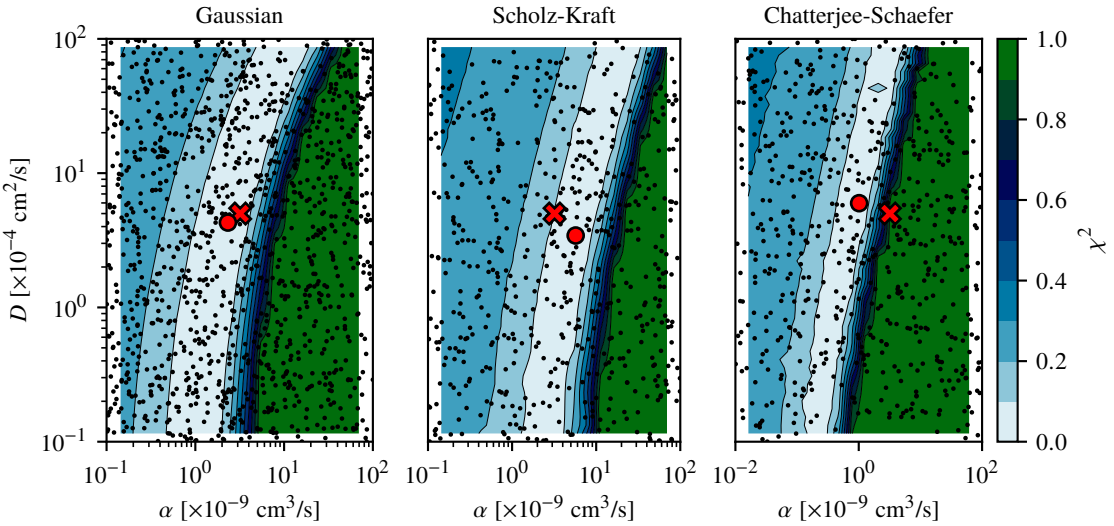

Figure 4: Maps over χ^2 from eq. (4) for various values of (α, D) for the three track structure models. Each dot represents a pair of (α, D) drawn from a uniform distribution. Only a fraction of the samples are shown. The literature value is marked with a cross in each case, whereas the (α, D) sets providing the best match to the experimental QCFs are marked with a closed circle and listed in table 2.

Table 2: The general parameters in the Blanc model providing the best fit to the experimental data: (i) when eq. (2) was truncated at the second-order term ($\beta = 0$) and (ii) including the third-order term ($\beta \neq 0$). The D value obtained from the χ^2 mapping in the second-order case (figure 4) was used in the third-order case (figure 5) as well.

		2nd order	3rd order	
Method	D [cm^2 s^{-1}]	α [cm^3 s^{-1}]	α [cm^3 s^{-1}]	β [cm^6 s^{-1}]
Literature	5×10^{-4}†	3.2×10^{-9}*	—	—
Gaussian	4.3×10^{-4}	2.3×10^{-9}	1.3×10^{-9}	9.1×10^{-27}
Scholz-Kraft	4.2×10^{-4}	5.7×10^{-9}	4.5×10^{-9}	2.7×10^{-27}
Chatterjee-Schaefer	5.9×10^{-4}	1.0×10^{-9}	6.1×10^{-10}	4.2×10^{-28}

† From Kallmann and Brucker (1957).
* Calculated from Birks (1964), *Kinetics of Quenching*, p. 199.

The third-order Blanc equation

The inclusion of the third-order β term in eq. (2) provides information about the local excitation density as trimolecular quenching requires a high-LET to occur. Adding higher-order terms in the Blanc model corresponds to extending the eq. (1) with additional terms, e.g. extending the Birks model to the Chou model and so on. The diffusion constant D is now fixed at the value obtained from minimizing χ^2 in figure 4, see table 2, to compare the magnitudes of the bi- and trimolecular quenching terms to each other for protons. The χ^2 maps for the Gaussian, Scholz-Kraft, and Chatterjee-Schaefer track structures are given in figure 5. The pair of (α, β) providing the best fit to the experimental data is given in table 2 and marked with a filled circle in figure 5. Henceforth, the three parameters D, α, and β as given in table 2 are used to compute the QCF for a given plastic scintillator.

4.2 Quenching correction factors

The measurements by Wang et al. (2012) of the quenched signal from the BCF-12 scintillator during proton irradiations are shown in figure 6, where the Birks model has been fitted to the data. The quenched response for the BCF-12 calculated with the Blanc model and the parameters in table 2 are shown alongside for each track structure model.

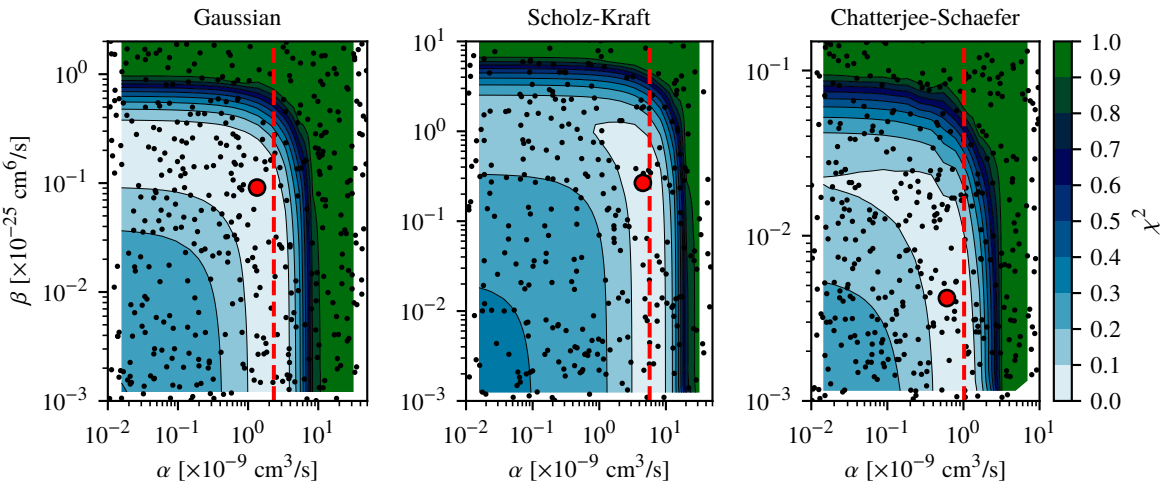

Figure 5: χ^2 maps when the parameter D is kept at the value given in table 2 and the quenching parameters α and β vary. Only a fraction of the samples are shown for simplicity. The dashed line corresponds to the α value obtained from figure 4, i.e. for $\beta \to 0$. The (α, β) values at the χ^2 minima are marked with a filled circle and listed in table 2.

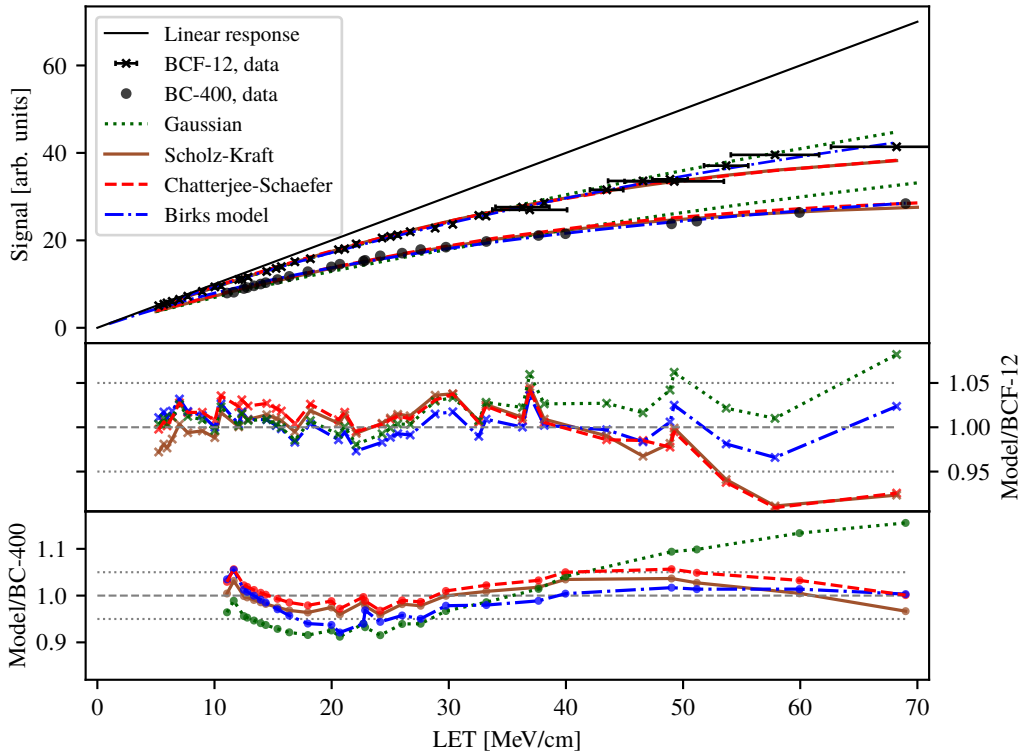

Figure 6: The quenched signals of the BCF-12 (Wang et al., 2012) and BC-400 (Torrisi, 2000) scintillators are plotted with crosses and circles, respectively. The Birks model has been fitted to each data set for comparison. The `ExcitonQuenching` computed responses for both scintillators using the three track structure models are shown with lines. The ratio of the response from each model to the experimental values are shown below for both scintillators.

The quenching signal from the BC-400 scintillator irradiated with protons at different energies is for comparison plotted in the same figure. The Birks model is again fitted to the experimental data, whereas the quenched signal is computed independently of the data using the Blanc model and its parameters in table 2 and the BC-400 properties in table 1.

5 Discussion

5.1 Quenching in the Blanc model

Second-order Blanc equation, $\beta = 0$. The χ^2 maps for the three track structure models in figure 4 indicate a distinct correlation between α and D, which also is evident from Birks (1964, p. 199), where α after several approximations is shown to be proportional to D. The mutual dependency indicates the primary role of the exciton diffusion constant: Due to the cylindrical symmetry of track structure models, the diffusion term $D\nabla^2 n$ effectively gives rise to exciton migration away from the center of the track. This in turns diminishes the bimolecular quenching rapidly as it is proportional to the square of the exciton density. Consequently, the quenching parameter α needs to increase if D increases to give rise to the same amount of quenching.

Third-order Blanc equation, $\beta \neq 0$. The χ^2 maps in figure 5 show the density dependence of the bi- and trimolecular quenching parameters α and β. As $\beta \to 0$, the α value providing the best match to the data converges towards the α value from figure 4 marked with a dashed line. The β value equivalently seems to converge for $\alpha \to 0$, as anticipated, although such a value is not of interest.

Nonetheless, all three χ^2 maps contain a ridge, where both the α and β terms contribute to the ionization quenching, which indicates that an extra term—as in the Chou model relative to the Birks model—may be relevant for high-LET situations. The pair of (α, β) providing the best fit to the experimentally determined QCFs, the minimum χ^2 value, is for the Gaussian and Scholz-Kraft track structure found around the χ^2 ridge. The χ^2 minima are overall in the proximity to $\beta \to 0$ indicating that the β term is close to be negligible for proton relevant LETs.

The β term is only relevant for high-LET cases and these are often associated with large uncertainties for protons, as in the present case, which makes an unambiguous conclusion on its importance for protons difficult. As such, the small effect of an extra quenching parameter is in line with the literature: Birks (1964, p. 194) investigated the extra parameter in the Chou model relative to the Birks model and concluded it redundant for the case of anthracene exposed to protons and α-particles. Torrisi (2000), on the other hand, concluded that the Chou model provides a better fit to the data for the BC-400 scintillator during proton irradiations than the Birks model does. The β term, or even additional terms of higher order, may be subject to a later investigation for particles with substantially higher LET than protons.

5.2 Ionization quenching correction factors

The QCF measurements by Wang et al. (2012) comprise several points between $5\,\mathrm{MeV\,cm^{-1}}$ and $70\,\mathrm{MeV\,cm^{-1}}$. However, more than half the measurements are below $25\,\mathrm{MeV\,cm^{-1}}$ and most measurements above $40\,\mathrm{MeV\,cm^{-1}}$ are associated with large uncertainties. In that light, it is not surprising that the three computed fluorescence signals in figure 6, including ionization quenching, are within few percent of the measurements for LET values up to $50\,\mathrm{MeV\,cm^{-1}}$ but deviate up to ±10 % for higher LET values.

The BC-400 has a light yield around 40 % larger than the BCF-12 scintillator, as is shown in table 1, and is thus in the Blanc model expected to give rise to a larger degree of quenching due to its larger initial exciton density. However, the ∼ 35 % lower scintillator decay time for the BC-400 in turn causes a faster fluorescence emission which reduces the quenching. Hence, the fluorescence emission in the BC-400 scintillator differs greatly from that of the BCF-12 scintillator and therefore serves as a means of testing the Blanc model.

The Blanc model with its fitted parameters is assessed against the BC-400 data by Torrisi (2000) in figure 6. The Scholz-Kraft and Chatterjee-Schaefer track structure models both predict the quenching signal within ±5 % of the measurements. The model-predicted signal divided by the measured signal in the lower part of the figure seems to contain the same structure in all four cases. On the other hand, the lack of a particle energy-dependent penumbral radius causes the Gaussian model to overestimate the ionization quenching for low-LET and vice versa for high-LET. The fact that the modified Blanc model follows the same structure as the Birks model in figure 6 was anticipated, as the Birks model is contained within and a simplified solution to the Blanc model as stated above. The agreement between `ExcitonQuenching` and the experimental data at high-LET in figure 6 is better for the BC-400 scintillator than for the BCF-12 scintillator. This might be explained by the fact, that Torrisi (2000) used thin scintillator pieces

which gave an excellent LET-resolution whereas the high-LET measurements by Wang et al. (2012) contain large uncertainties. Similarly for `ExcitonQuenching`, the uncertainties associated with the input parameters give rise to an uncertainty of the QCF. A ±2 % variation in the scintillator light yield for the BCF-12 scintillator changes the computed QCF about ±2 % for a proton with 50 MeV cm^{-1}. The similar variation of the light yield in the BC-400 scintillator exposed to the same proton energy however gives a variation about 4 % of the QCF due to its larger light yield.

Nonetheless, the excellent agreement within few percent between the Birks and Blanc models for especially the Chatterjee-Schaefer track structure validates the application of the Blanc model, as the results are calculated completely independently: The Birks model by fitting to the experimental data, whereas the Blanc model response is computed numerically by solving the partial differential equation with initial conditions given by the specific particle and plastic scintillator.

The Blanc model furthermore explains why the fluorescence emission in a PMMA-based optical fibre during proton irradiations is reported to be quenching-free (Jang et al., 2012; Christensen et al., 2018); The low light yield A in PMMA, relative to a traditional scintillator, gives rise to such a low initial linear exciton density ($n \propto A$) that $\alpha n^2 \approx \beta n^3 \approx 0$ in eq. (2) even for high-LET. Consequently, QCF $\simeq 1$ in the workflow in figure 3(c) corresponding to negligible quenching.

6 Conclusion

The open source software `ExcitonQuenching` combines amorphous track structure theory and the Blanc model to compute theoretical quenching correction factors for organic scintillators exposed to ions. Hence, it provides a new method—and more general than that due to Birks—to correct the ionization quenching from first principles which otherwise is a cumbersome experimental procedure.

The local exciton densities for proton relevant LETs are sufficient for bimolecular quenching to occur cf. figure 4 whereas the trimolecular quenching is almost vanishing for protons in the investigated water-equivalent materials. As a consequence, trimolecular quenching is not included in the online version of `ExcitonQuenching` but may be relevant for particles with higher LET in a later study.

The theoretically computed QCFs are compared to experimentally obtained QCFs for two plastic scintillators which differ greatly in their emission properties and thus quenching. The theoretical QCFs for the Scholz-Kraft and Chatterjee-Schaefer track structure models are within 3 % of the Birks model for low-LET and 5 % for high-LET for the BC-400 scintillator. The agreement between `ExcitonQuenching` and experimental data for the BCF-12 scintillator is within 2 % for LET-values below 45 MeV cm^{-1}, where the experimental uncertainties were small. The discrepancy however increases up to 10 % for the largest LET-values where the experimental measurements contain relative uncertainties of 8 %.

`ExcitonQuenching` depends on the density, decay time, and light yield of the scintillator, and thus constitutes a new method to compute QCFs for organic plastic scintillator exposed to ions without prior knowledge of the quenched scintillator response from experimental data.

Acknowledgements

The work was supported by the Danish Cancer Society and the Danish Council for Independent Research (grant FTP, DFF – 4184-00151). We thank Professor Lorenzo Torrisi for providing the original data of the luminescence response of the BC-400 scintillator during proton irradiations.

A Amorphous track structure models

Any track structure must satisfy $2\pi \int_0^\infty n(r)\, r\mathrm{d}r = N_0$. The three track structure models are compared for protons in water in figure 1 for two energies.

Gaussian: The Gaussian distribution is of the form

$$n_{\text{Gaussian}}(r, 0) = \frac{N_0}{\pi b^2} \exp\left(-\frac{r^2}{b^2}\right), \tag{5}$$

where $b = 2r_0/\sqrt{\pi}$ (Blanc et al., 1962). Birks (1964) sets $r_0 = 0.5 \times 10^{-6}$ cm, as obtained by Kallmann and Brucker (1957) for heavily ionizing particles. The main drawback of the Gaussian track structure is, that the energy-dependent

range of the secondary electrons is unaccounted for. Blanc et al. (1964) applied a Gaussian distribution to solve eq. (2) with $\beta = 0$ analytically using several approximations.

Scholz-Kraft: The Scholz-Kraft track structure models the energy deposition as a dense core of radius $r_{\min} = 0.01\,\mu\text{m}$ which falls off proportionally to r^{-2} until the maximum range of the secondary electrons

$$r_{\max} = 0.05\,\mu\text{m}\,\text{MeV}^{-1.7} \times E^{1.7}$$

has been reached:

$$n_{\text{SK}}(r) = \begin{cases} \dfrac{N_0}{r_{\min}^2}\left(\pi\left[1 + 2\,\ln\dfrac{r_{\max}}{r_{\min}}\right]\right)^{-1} & \text{for} \quad r < r_{\min} \\ \dfrac{N_0}{r^2}\left(\pi\left[1 + 2\,\ln\dfrac{r_{\max}}{r_{\min}}\right]\right)^{-1} & \text{for} \quad r_{\min} \le r \le r_{\max} \\ 0 & \text{for} \quad r > r_{\max} \end{cases} \tag{6}$$

Chatterjee-Schaefer: The Chatterjee-Schaefer model has a denser core than the Scholz-Kraft model with radius

$$r_{\min} = r_{\text{core}}\,\beta_{\text{ion}}, \tag{7}$$

where $r_{\text{core}} = 11.6\,\text{nm}$ and $\beta_{\text{ion}} = v/c$ is the ratio of the speed v to the speed of light c. The outer border of the penumbra has a radius of

$$r_{\max} = 0.768\,\mu\text{m}\,\text{MeV}^{-1} \times E - 1.925\,\mu\text{m}\,\text{MeV}^{-0.5} \times \sqrt{E} + 1.257\,\mu\text{m}$$

and will consequently give rise to a relatively large amount of ionization quenching in the core:

$$n_{\text{CS}}(r) = \begin{cases} \dfrac{N_0}{2\pi r_{\min}^2} + \dfrac{N_0}{4\pi r_{\min}^2}\left(\ln\left(\sqrt{e}\dfrac{r_{\max}}{r_{\min}}\right)\right)^{-1} & \text{for} \quad r < r_{\min} \\ \dfrac{N_0}{4\pi r^2}\left(\ln\left(\sqrt{e}\dfrac{r_{\max}}{r_{\min}}\right)\right)^{-1} & \text{for} \quad r_{\min} \le r \le r_{\max} \\ 0 & \text{for} \quad r > r_{\max} \end{cases} \tag{8}$$

with more than half the excitations inside the core. The Scholz-Kraft and Chatterjee-Schaefer models are developed for water and thus the core and penumbra radii are scaled with the density of the water-equivalent plastic scintillator in question.

B Numerical scheme

The cylindrical symmetry of the track structure models reduces the problem to be one dimensional; the LET of the ion along its path is constant on the microscopical scale, which in turns causes the second derivative of the excitation density in eq. (2) to vanish along the trajectory, and only the radial diffusion is left.

The one dimensional mesh of length $L = 2r_{\max}$, where the ion trajectory is centred, defines the solution domain. The distance between two neighbouring voxels Δx is limited by $\Delta x < r_{\min}/l$, where $l > 1$ is chosen to satisfy the natural requirement, that a numerical integration over the excitation densities in the mesh grid must equal the analytical integration. For the Scholz-Kraft and Chatterjee-Schaefer track structures, $l > 20$ turned out fulfil the said requirement, whereas $\Delta x < r_0/5$ was sufficient for the Gaussian case.

The explicit Lax-Wendroff scheme (Lax and Wendroff, 1960) is applied to solve the partial differential equation. The derivatives of the exciton density n_i^m for voxel $i \in [1, 2, \ldots, L/\Delta x - 1]$ at time step m are

$$\left.\frac{\partial n}{\partial t}\right|_i^m \simeq \frac{n_i^{m+1} - n_i^m}{\Delta t} \quad \text{and} \quad \left.\frac{\partial^2 n}{\partial x^2}\right|_i^m \simeq \frac{n_{i+1}^m - 2n_i^m + n_{i-1}^m}{(\Delta x)^2}.$$

The time step Δt is subject to the von Neumann stability conditions (Press et al., 1988; Dehghan, 2004). The open-source code library `libamtrack` (Toftegaard et al., 2014) is used to calculate the LET and β_{ion} in eq. (7) depending on the particle energy.

References

Alsanea F, Therriault-Proulx F, Sawakuchi G, and Beddar S. 2018 A real-time method to simultaneously measure linear energy transfer and dose for proton therapy using organic scintillators *Med. Phys.* **45** 1782–89

Archambault L, Beddar A S, Gingras L, Roy R, and Beaulieu L 2005 Measurement accuracy and Cerenkov removal for high performance, high spatial resolution scintillation dosimetry *Med. Phys.* **33** 128–35

Beddar A S, Mackie T R, and Attix F H 1992a Water-equivalent plastic scintillation detectors for high-energy beam dosimetry: I. Physical characteristics and theoretical considerations *Phys. Med. Biol.* **37** 1883–900

Beddar A S, Mackie T R, and Attix, F H 1992b Water-equivalent plastic scintillation detectors for high-energy beam dosimetry: II. Properties and measurements *Phys. Med. Biol.* **37** 1901–13

Beddar S and Beaulieu L 2016 *Scintillation Dosimetry* CRC Press

Birks J B 1951 Scintillation from organic crystals: Specific fluorescence and relative response to different radiation *Proc. Phys. Soc A* **64** 874–7

Birks J B 1964 *The Theory and Practice of Scintillation Counting: International Series of Monographs in Electronics and Instrumentation* volume 27 Elsevier

Blanc D, Cambou F and Lafond Y G D 1962 Kinetics of the fast component of scintillation in a pure organic medium. Application to anthracene *Comptes rendus de l'Académie des Sciences Paris* **18** 3187–9

Blanc D, Cambou F and Lafond Y G D 1964 Etude cinétique de la scintillation dans les cristaux organiques purs *Journal de Physique* **25** 319–25

Boivin J, Beddar S, Bonde C, Schmidt D, Culberson W, Guillemette M, and Beaulieu L 2016 A systematic characterization of the low-energy photon response of plastic scintillation detectors *Phys. Med. Biol.* **61** 5569–86

Buranurak S, Andersen C E, Beierholm A R, and Lindvold L R 2013 Temperature variations as a source of uncertainty in medical fiber-coupled organic plastic scintillator dosimetry *Rad. Meas.* **56** 307–11

Chatterjee A and Schaefer H J 1976 Microdosimetric structure of heavy ion tracks in tissue *Rad. Environm. Biophys.* **13** 215–27

Chou C N 1952 The Nature of the Saturation Effect of Fluorescent Scintillators *Phys. Rev.* **5** 904–5

Christensen J B, Almhagen E, Nyström H, and Andersen C E 2018 Quenching-free fluorescence signal from plastic-fibres in proton dosimetry: understanding the influence of Čerenkov radiation *Phys. Med. Biol.* **63** 065001

Dehghan M 2004 Numerical solution of the three-dimensional advection – diffusion equation *Applied Mathematics and Computation* **150** 5–19

Hansen J W and Olsen K J 1984 Experimental and Calculated Response of a Radiochromic Dye Film Dosimeter to High-LET Radiations *Rad. Research* **97** 1–15

Hoer C, Lindsay C, Beaudry J, Penner C, Strgar V, Lee R and Duzenli C 2018 Characterization of the exradin W1 plastic scintillation detector for small field applications in proton therapy *Phys. Med. Biol.* **63** 095016

Jang K W, Yoo W J, Shin S H, Shin D and Lee B 2012 Fiber-optic Čerenkov radiation sensor for proton therapy dosimetry *Optics Express* **20** 13907–14

Kallmann H and Brucker G J 1957 Decay Times of Fluorescent Substances Excited by High-Energy Radiation *Phys. Rev.* **108** 1122–30

Katz R and Varma M N 1991 *Radial distribution of dose* Springer Boston 163–80

Kiefer J and Straaten H 1986 A model of ion track structure based on classical collision dynamics *Phys. Med. Biol.* **31** 1201–09

Lax P and Wendroff B 1960 Systems of Conservation Laws *Communications on pure and applied mathematics* 217–37

Michaelian A and Menchaca-Rocha A 1994 Ion-Induced Luminescence Based on Energy Deposition *Phys. Rev. B* **49** 550–62

Newman E and Steigert F E 1960 Response of NaI(Tl) to Energetic Heavy Ions *Phys. Rev.* **118** 1575–78

Press W H, Teukolsky S A, Vetterling W T and Flannery B P 1988 *Numerical Recipes in C The Art of Scientific Computing* Cambridge University Press

Saint-Gobain 2018 Scintillating fibres `https://www.crystals.saint-gobain.com/products/scintillating-fiber`

Scholz M and Kraft G 1996 Track structure and the calculation of biological effects of heavy charged particles *Adv. Space Res.* **18** 5–14

Therriault-Proulx F, Beddar S, Briere T M, Archambault L and Beaulieu L 2011 Technical Note: Removing the stem effect when performing Ir-192 HDR brachytherapy *in vivo* dosimetry using plastic scintillation detectors: A relevant and necessary step *Med. Phys.* **38** 2176–79

Toftegaard J, Lühr A, Sobolevsky N, and Bassler N 2014 Improvements in the stopping power library `libdEdx` and release of the web GUI `dedx.au.dk` *Journal of Physics: Conference Series* **489** 012003

Torrisi L 2000 Plastic scintillator investigations for relative dosimetry in proton-therapy *Nucl. Instrum. Methods Phys. Res.* **170** 523–30

Wang L L, Perles L A, Archambault L, Sahoo N, Mirkovi D and Beddar S 2012 Determination of the quenching correction factors for plastic scintillation detectors in therapeutic high-energy proton beams *Phys. Med. Biol.* **57** 7767–81

Wootton L and Beddar S 2013 Temperature dependence of BCF plastic scintillation detectors *Phys. Med. Biol.* **58** 2955–67